

Article

Negative Temperature Coefficient of Resistance in Aligned CNT Networks: Influence of the Underlying Phenomena

Stepan V. Lomov ¹, Iskander S. Akmanov ¹, Qiang Liu ², Qi Wu ² and Sergey G. Abaimov ^{1,*}

¹ Center for Petroleum Science and Engineering, Skolkovo Institute of Science and Technology, Bolshoy Boulevard 30 bld. 1, Moscow 121205, Russia

² State Key Laboratory of Mechanics and Control of Mechanical Structures, Nanjing University of Aeronautics and Astronautics, Nanjing 210016, China

* Correspondence: s.abaimov@skoltech.ru

Abstract: Temperature dependence of electrical conductivity/resistivity of CNT networks (dry or impregnated), which is characterised by a temperature coefficient of resistance (TCR), is experimentally observed to be negative, especially for the case of aligned CNT (A-CNT). The paper investigates the role of three phenomena defining the TCR, temperature dependence of the intrinsic conductivity of CNTs, of the tunnelling resistance of their contacts, and thermal expansion of the network, in the temperature range 300–400 K. A-CNT films, created by rolling down A-CNT forests of different length and described in Lee et al., *Appl Phys Lett*, 2015, 106: 053110, are investigated as an example. The modelling of the electrical conductivity is performed by the nodal analysis of resistance networks, coupled with the finite-element thermomechanical modelling of network thermal expansion. The calculated TCR for the film is about -0.002 1/K and is close to the experimentally observed values. Comparative analysis of the influence of the TCR defining phenomena is performed on the case of dry and impregnated films. The analysis shows that in both cases, for an A-CNT film at the studied temperature interval, the main factor affecting a network's TCR is the TCR of the CNTs themselves. The TCR of the tunnelling contacts plays the secondary role; influence of the film thermal expansion is marginal. The prevailing impact of the intrinsic conductivity TCR on the TCR of the film is explained by long inter-contact segments of CNTs in an A-CNT network, which define the homogenised film conductivity.

Keywords: carbon nanotubes; electrical conductivity; temperature coefficient of resistance; coefficient of thermal expansion



check for updates

Citation: Lomov, S.V.; Akmanov, I.S.; Liu, Q.; Wu, Q.; Abaimov, S.G.

Negative Temperature Coefficient of Resistance in Aligned CNT Networks: Influence of the Underlying Phenomena. *Polymers* **2023**, *15*, 678. <https://doi.org/10.3390/polym15030678>

Academic Editor: Lisa Rita Magnaghi

Received: 30 November 2022

Revised: 18 January 2023

Accepted: 19 January 2023

Published: 29 January 2023



Copyright: © 2023 by the authors. Licensee MDPI, Basel, Switzerland. This article is an open access article distributed under the terms and conditions of the Creative Commons Attribution (CC BY) license (<https://creativecommons.org/licenses/by/4.0/>).

1. Introduction

Temperature coefficient of resistance (TCR) is defined as:

$$\text{TCR} = \frac{1}{R} \frac{dR}{dT} = -\frac{1}{G} \frac{dG}{dT}; \quad R = \frac{1}{G} \quad (1)$$

where R is electrical resistance (or resistivity), G is electrical conductance (or conductivity), and T is temperature.

The TCR of carbon nanotube (CNT) networks in films and nano-composites has been studied during last two decades. In the temperature range of 300–400 K, important for many applications of CNT-based sensors, negative TCRs are widely reported for random and aligned CNT configurations for practically attainable CNT volume fractions [1–11]. Apart from sensing, TCR may be relevant for other applications exploiting high electric conductivity of CNTs [12,13].

Three factors can affect the temperature dependence of the homogenised conductivity: (1) changes with temperature in intrinsic conductivity of CNTs, (2) changes with temperature in potential barriers at CNT contacts, influencing tunnelling conductance of these

contacts, (3) configurational changes in the CNT network due to differences in coefficients of thermal expansion (CTE), influencing lengths of CNT segments between contacts and tunnelling distances. The comparative influence of these factors on the homogenised TCR is difficult to be derived from direct experiments due to the impossibility of separating involved phenomena. The problem can be approached using certain interpretations of the trends in macro-level measurements [8] or by the modelling of CNT resistive networks [9,10,14]. These modelling studies focus on the dependency of the homogenised TCR on morphological features of a CNT network, such as CNT volume fraction, orientation, and length distributions. The comparative effect of the underlying physical phenomena is investigated rather superficially. Moreover, the key parameters of the models, such as the TCR value of a single CNT, that determine the result are often chosen arbitrarily.

The present paper investigates the comparative effects for an example of CNT films, studied in [8]. As described in [8], aligned CNT (A-CNT) arrays with varying CNT length were grown in a quartz tube furnace at atmospheric pressure via a thermal catalytic chemical vapor deposition process, and re-oriented and densified using a 10 mm diameter rod and Teflon film by rolling in the alignment direction.

All properties are investigated in a temperature range of 300–400 K. The sheet resistance was evaluated using a four-point probe method (Keithley SCS-4200) where electrode–CNT connections were established using Ag paint. For the details of the films fabrication and the measurements, the reader is referred to [8].

Ref. [8] provided detailed experimental data on the sheet resistance of the films, allowing the identification of the parameters of the A-CNT geometry followed by the modelling of films' internal structure, generating the data for the comparative study in the present paper. The A-CNT network geometry is used for the analysis of network's TCR in the case of non-impregnated film (compared with the experimental data in [8]), and in the case of the film, impregnated with epoxy matrix.

2. A-CNT Films and Identification of the Nano-Structure Parameters

The parameters of multi-walled CNTs (MWCNTs), as described in [8], are shown in Table 1. The input parameters of the CNT geometry generator (maximal curvature and torsion) for similar A-CNTs were validated in [15]. These parameters are directly implemented in the modelling of our study.

Table 1. Parameters of CNTs and the CNT film.

Group	Parameter	Value
Defined in [8,15]	Wall count	5
	CNT outer diameter D , nm	7.78
	CNT inner diameter, nm	5.12
	CNT volume fraction $V_{F_{grown}}$, as grown	1.6%
	CNT length (L) range, μm	100–500
	Maximal CNT curvature κ_{max} , $1/\mu\text{m}$	15
	Maximal CNT torsion τ_{max} , $1/\mu\text{m}$	10
	Thickness of the rolled-down CNT film t , indicative, μm	10
Identified by fitting the resistance/length dependency in [8]	CNT intrinsic conductivity g_{intr} , S/m	$2 \cdot 10^6$
	Tunnelling barrier ΔE in vacuum, eV	3
	Tunnelling barrier ΔE above the polymer cutoff distance, eV	2
	Inclination angle α^*	55°

As described in [8], the vertical A-CNT forest has an original thickness of $H = L/1.5$, where L is the CNT length. Next, it is rolled down to the thickness of $\sim 10 \mu\text{m}$. After this process, the film will have a fibre volume fraction of:

$$VF = VF_{grown} \frac{L}{1.5t} \quad (2)$$

where VF_{grown} is CNT “as grown volume fraction”, and t is the indicative thickness of the rolled down film (see Table 1).

After the rolling, the CNTs in the film are not parallel to the substrate but are inclined, as is clearly seen in Figure 1a. The details of the resulting geometrical configuration were not investigated in [8], but they can be “reversely engineered” based on the dependency of the sheet resistivity of the films on the CNT length, given in [8].

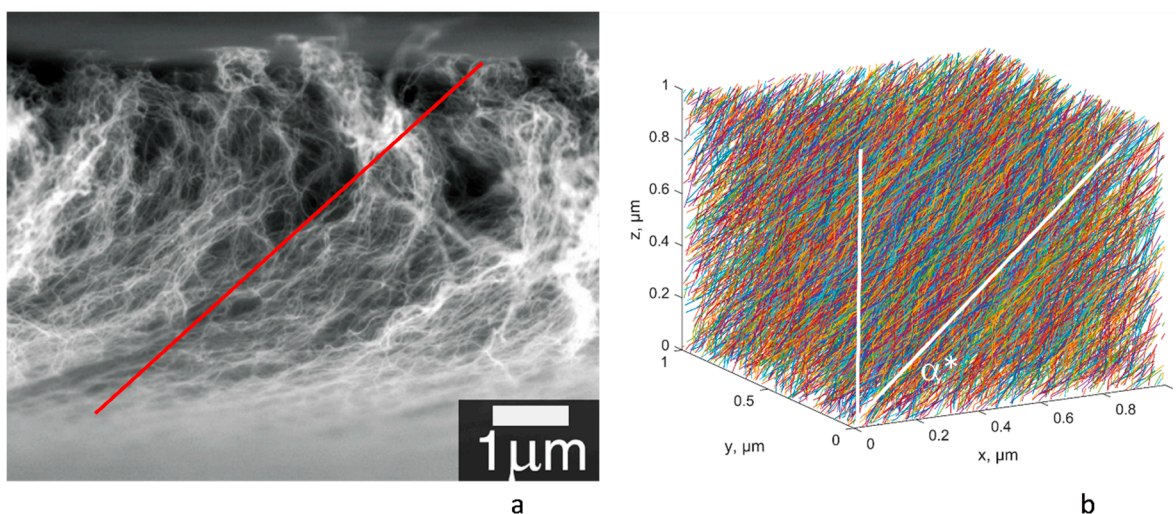


Figure 1. Geometry of the A-CNT film: (a) SEM of the film after rolling down. Reproduced with permission from Ref. [8]. Copyright 2023, AIP Publishing; (b) RVE of the model, CNT length $100 \mu\text{m}$, $\alpha^* = 55^\circ$. The red line in (a) corresponds to the assumed inclination α^* .

As a simplification, we assume that after rolling, the CNTs have a prevailing orientation α^* (Figure 1b) and build a random configuration of the representative volume element (RVE), as briefly described in Appendix A, using the CNT parameters given in Table 1. The details of the geometric algorithm can be found in [15,16]. The RVE of size $1 \times 1 \times 1 \mu\text{m}$ is generated. This is performed for three variants of CNT length: $L = 100, 250, \text{ and } 500 \mu\text{m}$. The corresponding CNT volume fractions, according to Equation (2), are 11%, 27%, and 53%, respectively. An example of a generated RVE is shown in Figure 1b.

The conductivity of the RVE is homogenized using the transformation of the geometrical model into a network of resistances and nodal analysis of the resulting electrical scheme, as briefly described in Appendix A. These calculations are performed for CNT electrical parameters at reference (room) temperature, taken as $T_R = 300 \text{ K}$. In the experiments [8], two components of the anisotropic sheet resistance were measured: R_0 along the CNT rolling direction (x in Figure 1b) and R_{90} in the cross direction (y in Figure 1b). For comparison with the results of calculations, the sheet resistance values can be transformed into components of the homogenized conductivity tensor as:

$$g_{xx} = \frac{1}{tR_0}; g_{yy} = \frac{1}{tR_{90}} \quad (3)$$

corresponding to directions x, y in Figure 1b.

The conductance of the elements of the network at T_R is calculated using the following formulae:

- Conductance of CNT connections between the contact points:

$$G(l) = g_{intr} \frac{\pi D^2 / 4}{l} \quad (4)$$

where D is the CNT outer diameter (see Table 1), l is the inter-contact CNT length, and g_{intr} is the intrinsic conductivity of the CNT.

- Tunnelling conductance of the CNT contact: Simmons' formula [17,18]:

$$G_{tunn} = G_0 \frac{\tau D^2}{s^2} \mathfrak{F}; \quad \mathfrak{F} = \exp(-\tau s) \quad (5)$$

where s is the contact distance between CNT surfaces, $s \geq s_{min} = 0.34$ nm, $G_0 = 2e^2/h = 7.722 \cdot 10^{-5}$ S ($e = 1.602 \cdot 10^{-19}$ C is electron's charge, $h = 6.626 \cdot 10^{-34}$ J·s is Planck's constant), and the tunnelling constant:

$$\tau = \frac{4\pi\sqrt{2m\Delta E}}{h} \quad (6)$$

where $m = 9.109 \cdot 10^{-31}$ kg is electron's mass and ΔE is the potential barrier.

For the dry network (vacuum is assumed), the tunnelling constant is about 20 nm^{-1} [19], which gives ΔE about 3 eV. This value is assumed for calculations (see Table 1). In the case of the absence of polymer in the tunnelling contact, there is no "polymer cutoff" effect [20]; hence, one value ΔE is used for any contact distance. When impregnated film is considered, the polymer cutoff distance of 0.6 nm is used, and for $s > 0.6$ nm the value $\Delta E = 2$ eV is used [20].

The CNT minimal contact distance can, in principle, be affected by CNT compression. The effect of this on the homogenized conductivity was evaluated in [21] and found to be weak; therefore, the value of 0.34 nm is retained in the present calculations.

In the geometrical/electrical model, described above, there are parameters, which should be chosen to fit the experimentally determined sheet resistance:

- Intrinsic conductivity g_{intr} in Equation (4), which defines the level of the homogenised conductivity and hence the sheet resistance (both its components);
- Angle α^* , which also affects the values g_{xx} and g_{yy} , but most importantly defines the ratio $g_{xx}/g_{yy} = R_{90}/R_0$, which was found to be close to 1.4 in experiments [8].

In [21], the present authors compared the influence of parameters defining different conductance mechanisms and found that g_{intr} is the most influential one and has to be fitted in the first place. When this was completed, the use of most common values for the tunnelling resistance and inter-CNT contact distance gave good correspondence with the experimental measurements in [8].

The dependency of film conductivity on CNT length, $g_{ii}(L)$, is largely defined by the change in CNT volume fraction, according to Equation (2).

The fitting process of experimental data vs. numerical predictions resulted in the parameters shown in Table 1. Figure 2 shows the results of the calculation of the film conductivity components with input parameters given in Table 1. The experimental points are calculated using Equation (3), and the sheet resistance data presented in [8]. The good correspondence with the experimentally measured values and $g_{ii}(L)$ linear trends shows that the assumptions made in the formulation of the model and the choice of model parameters were correct.

Notably, the dependence $g_{ii}(L)$ is close to linearity. The R^2 values of the linear fit for g_{xx} and g_{yy} are 0.85 and 0.87, respectively; when fitting with a power law $g_{ii} \propto L^{\alpha_{ii}}$, the values of α are equal to 0.89 for both curves and the R^2 values are also 0.85 and 0.87. The difference between the linear fit and the power law fit values is 2% or less (the power law fits are not presented in Figure 2 because they are nearly indistinguishable visually from the linear fits).

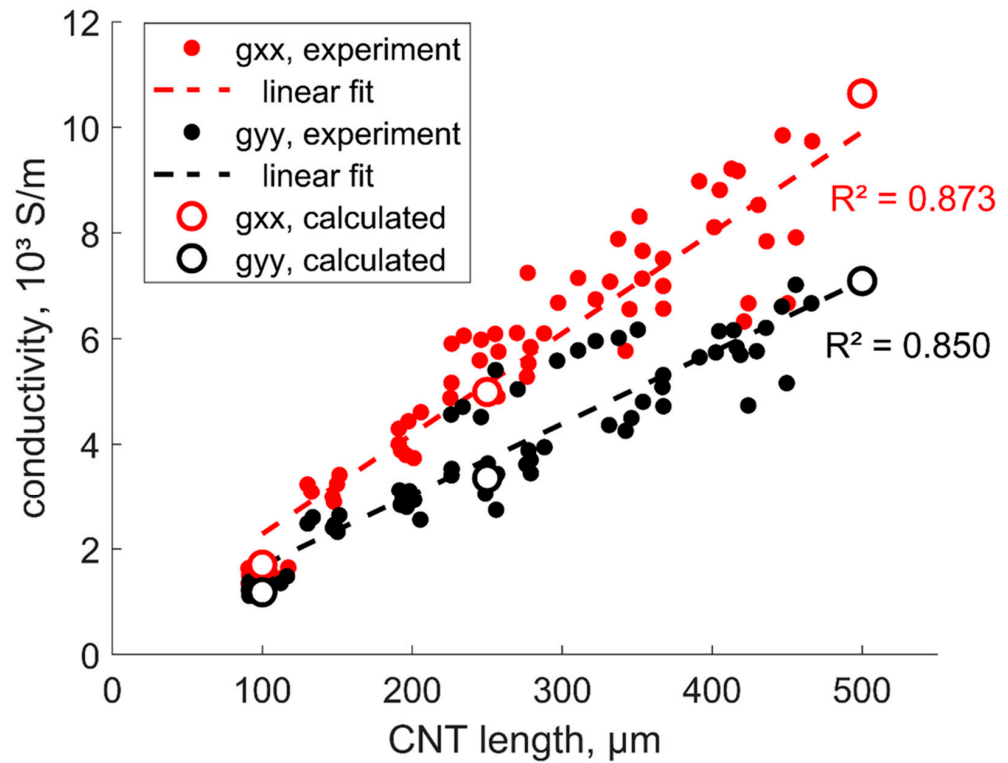


Figure 2. Components of the film conductivity in function of the CNT length, experiment [8] and calculations, average of results for ten random RVEs, and the size of circles corresponds to the scatter in the random simulations. R^2 values correspond to the linear fit.

Hence, (see Equation (2)) the dependence $g_{ii}(VF)$ is also close to linear. Two factors, intrinsic CNT conductivity and tunnelling conductivity of CNT contacts, both influence the $g_{ii}(VF)$ dependency in different ways. For aligned CNT geometry, the input of the intrinsic CNT conductivity into the homogenised film conductivity value should be roughly proportional to VF (increase in the number of the parallel conductors). The tunnelling conductivity influences the homogenised one via the number of CNT contacts in the network; this number in a simplified theory of fibrous assemblies is proportional to VF^2 [22,23]; actually, in the aligned RVEs, which are generated in the present work, the dependency is VF^α , $\alpha = 1.2$ (the calculation method is the same as in [21]).

The closeness of the dependence $g_{ii}(VF)$ to linearity suggests that the prevailing influence of the intrinsic CNT conductivity on the homogenized conductivity of the film will be reflected in the relative importance of different phenomena, defining the temperature dependence of the film conductivity.

3. Phenomena Defining the Temperature Dependence of Resistance

The temperature dependence of material resistivity (conductivity) is characterised with temperature coefficient of resistance.

If a change over a temperature interval $\Delta T = T - T_R$ is being considered, and derivatives in Equation (1) are changed to differences, then resistance (conductance) dependency on temperature is given by:

$$R(T) = R(T_R) \left(1 + \overline{TCR(T)} \cdot \Delta T \right); G(T) = \frac{G(T_R)}{1 + \overline{TCR(T)} \cdot \Delta T}; \Delta T = T - T_R \quad (7)$$

where $\overline{TCR(T)}$ is effective TCR over the interval (T_R, T) , $\overline{TCR(T)} = \frac{(R(T) - R(T_R))}{R(T_R) \Delta T}$.

3.1. Intrinsic Conductivity of CNTs

Different values for TCR of CNT intrinsic conductivity are given in the literature. For example, for MWCNTs and the temperature range 300–400 K [10,24] use the value 30 ppm/K = $3 \cdot 10^{-5}$ 1/K (positive); Ref. [14]—the value -0.002 1/K (negative). The contradiction is resolved when physically based formulae [25,26] are used to characterise temperature dependency of intrinsic conductivity.

Refs. [25,26] define a “neutral length”, L_N , as follows: if a CNT length $l = L_N$ is considered, then resistance of it is independent of temperature: “for $l < L_N$, the number of conduction channels is the dominant parameter determining the overall resistance, and increasing temperature lowers resistance; for $l > L_N$, electron mean free path is more important, and raising temperature increases resistance”. The neutral length is calculated as:

$$L_N = \frac{10^3 a T_0 D^2}{b + 2a T_0 D} \tag{8}$$

where $T_0 = 100$ K, $a = 2.04 \cdot 10^{-4}$ nm⁻¹K⁻¹, $b = 0.425$. For $D = 7.78$ nm (Table 1), $L_N = 1.66$ μm, which is much longer than a typical inter-contact distance in the considered CNT films, which is well below 1 μm. Therefore, in the present calculations, TCR of the CNT sections between the contacts will be negative.

The value of TCR for an MWCNT section of length l , using formulae in [25,26] and Equation (4), is calculated in the temperature interval 270–420 K as:

$$TCR_{CNT}(T) = \frac{1}{R_*} \frac{\pi D^2}{4} \frac{R_0}{10^3 D} \frac{2aD + b/T_0}{(aTD + b)^2} \left(1 - \frac{l}{L_N}\right) \tag{9}$$

where $R_0 = 1/G_0 = 1.29 \cdot 10^{-4}$ Ohm, $R_* = 2.5 \cdot 10^5$ S/m. This value R_* is chosen to fit the graphs shown in [25,26]. Following Equation (9), Figure 3a shows the dependency of a CNT section TCR on the section length for three levels of temperature. The dependency of TCR on T is weak (on the logarithmic scale): with the change in temperature from 300° K to 400° K TCR value changes by ~60%. As expected, for the section length below 1 μm, the value of TCR is negative.

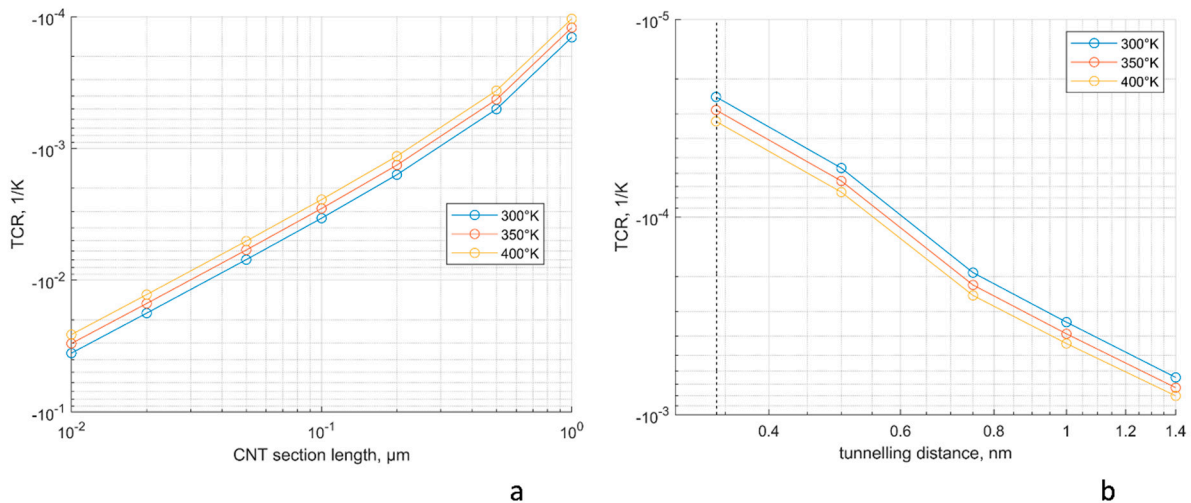


Figure 3. TCR for CNT sections and CNT contacts: (a) TCR of a CNT section, Equations (8) and (9); (b) TCR of a tunnelling contact due to thermal excitation; the dashed line indicates the minimum distance between the CNTs to be 0.34 nm.

Most of the inter-contact section lengths in the present models of RVE are about 0.1 μm in length; hence, TCR values will be of the order of -0.003 1/K. Note that the RVE has

translational periodicity symmetry, and the inter-contact length for CNT sections crossing the RVE faces should be calculated between the contacts in two neighbouring RVEs.

3.2. Tunnelling Conductance of CNT Contacts

Temperature dependence of the tunnelling resistance can be calculated using the formulae in [9–11], which express the presence of the thermally assisted tunnelling due to the excited levels of tunnelling across the barrier [27]. The higher the temperature is, the higher the electron energy is comparative to the barrier height, generating higher probabilities to overcome it, and thereby facilitating easier tunnelling. Later, to distinguish this mechanism from others, we will refer to it as “thermal excitation of tunnelling”. The conductance at temperature T will be expressed as [9–11]:

$$G_{tunn}(T) = G_{tunn}(T_R) \left(1 + \frac{\pi^2}{6} \left(\frac{k_B T}{\Delta E} \right)^2 \ln \mathfrak{J} (\ln \mathfrak{J} + 1) \right) \quad (10)$$

where $G_{tunn}(T_R)$ is the conductance given by Equations (5) and (6) at the reference temperature and $k_B = 1.380649 \times 10^{-23} \text{ m}^2 \text{ kg s}^{-2} \text{ K}^{-1}$ is Boltzmann’s constant. Differentiating Equation (10) and using Equation (1), the formula for TCR is derived:

$$TCR_{tunn}(T) = - \frac{2T \frac{\pi^2}{6} \left(\frac{k_B}{\Delta E} \right)^2 \ln \mathfrak{J} (\ln \mathfrak{J} + 1)}{1 + \frac{\pi^2}{6} \left(\frac{k_B T}{\Delta E} \right)^2 \ln \mathfrak{J} (\ln \mathfrak{J} + 1)} \quad (11)$$

Figure 3b shows the dependency of thermal excitation TCR for a CNT contact on the tunnelling distance for three levels of temperature. The most often occurring contact distances are near the minimal distance of 0.34 nm [23]; hence, TCR values will be of the order of $-3 \cdot 10^{-5} \text{ 1/K}$, i.e., two orders of magnitude smaller than TCRs for CNT sections.

3.3. Thermal Expansion

Thermal expansion of the impregnated CNT film is calculated using Abaqus finite element (FE) modelling. The geometry of CNTs in an RVE is transferred to Abaqus. Thermo-mechanical simulation was performed using coupled temperature-displacement analysis. CNTs are represented as trusses with a stiffness of 570 GPa (calculated based on the wall stiffness of 1 TPa) and $CTE_{CNT} = 20 \text{ ppm/K}$ [28], which are embedded in the matrix mesh. Embedded elements were widely used by the authors in their previous work on CNT composites modelling [29–31], as well as by others [32]. For the dry CNT film, the calculations are performed in the same manner but using zero CTE for the matrix and a very low Young’s modulus of 0.001 Pa. The boundary conditions in both cases are set according to [33].

As a result of calculations of changes in CNT network under the thermal expansion of both the CNTs and matrix, the distances between the points on CNT centrelines, corresponding to the contact positions, change from d in undeformed configuration to d_{TE} after the thermal expansion. This change will be characterised by the effective thermal expansion coefficient of the inter-centreline contact distance or CTE_d :

$$CTE_d = \frac{d_{TE} - d}{d \cdot \Delta T} \quad (12)$$

The tunnelling resistance/conductance is defined via Equations (5) and (6) by the inter-surface distance of the CNTs in the undeformed s and deformed s_{TE} configuration:

$$s = \max(s_{min}, d - D) \quad (13)$$

$$s_{TE} = \max(s_{min}, d_{TE} - D(1 + CTE_{CNT} \Delta T)) \quad (14)$$

where $s_{min} = 0.34 \text{ nm}$ is the minimal (van der Waals’) distance in between CNTs surfaces.

The corresponding effective thermal expansion coefficient of the inter-surface contact distance CTE_s :

$$CTE_s = \frac{s_{TE} - s}{s \cdot \Delta T} \tag{15}$$

Figure 4 illustrates the calculated effective CTE of tunnelling contacts for one random realisation of the RVE, CNT length 100 μm . The behaviour in the cases of $L = 250 \mu\text{m}$ and $L = 500 \mu\text{m}$ are analogous.

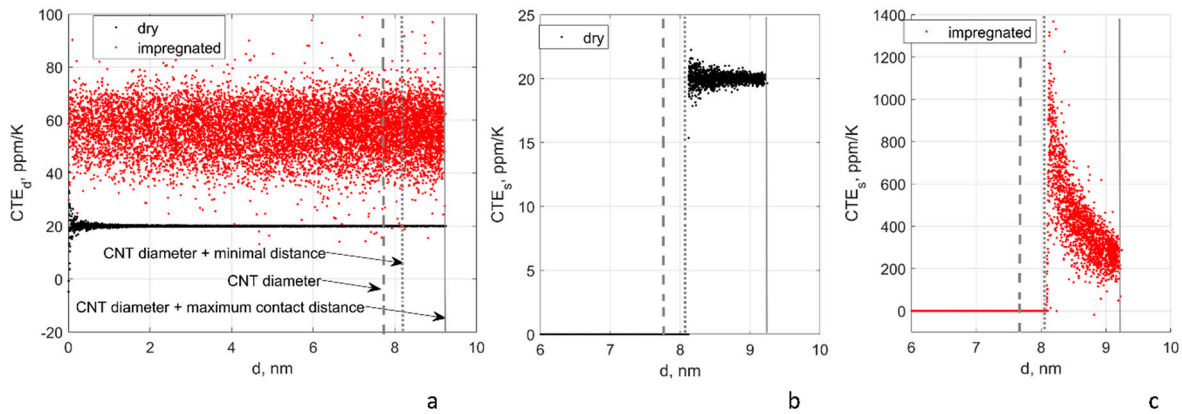


Figure 4. Effective CTE of the tunnelling contacts in function of the distance between the centrelines in the undeformed configuration: (a) CTE_d , dry, and impregnated film; (b,c) CTE_s , dry (b), and impregnated (c) film. CNT length 100 μm .

The values of the inter-centreline distance, CTE_d , characterise the FE modelling of the thermal expansion. For the impregnated film, $CTE_d = 56.4 \pm 9.6$ ppm/K (mean and standard deviation). The film expands with the mean CTE, which is a result of homogenisation of the matrix’s and CNTs’ CTEs with variations, given by the local CNT configuration.

For the dry film, $CTE_d = 20.0 \pm 1.1$ ppm/K for all the range of inter-centreline distances, and $CTE_d = 20.0 \pm 0.03$ ppm/K for $d > D + s_{min}$, the same behaviour of the “expanding film”.

In the embedded elements formulation, with the matrix mesh size larger than the inter-CNT contact distance, the nodes of the two contacting CNT may be kinematically linked to the same matrix node. This will create a numerical effect of a certain link between the CNTs, even with the very weak matrix. The CNTs in the film do not, therefore, behave as a “heap of sticks”, expanding independently. The “expanding film” behaviour can be seen as an imitation of physical phenomena of the CNT interaction caused by, for example, friction under normal forces, created by the CNT curvature and compression in the contacts [23]. Of course, this remains an heuristic explanation; full description of the contact behaviour would require a precise definition of the non-interpenetrating CNT volumes and solving the corresponding contact problems, as is performed for fibrous assemblies [34].

The transition from CTE_d to CTE_s can be understood if CTE_d is represented for a certain contact as:

$$CTE_d = CTE_{dmean}(1 + \epsilon) \tag{16}$$

where $CTE_{dmean} = 56$ ppm/K for impregnated and 20 ppm/K for the dry film, where ϵ can be positive or negative. Evaluating ϵ as coefficients of variation for CTE_d of dry and impregnated film, $|\epsilon| \sim 0.2$ and ~ 0.00015 , respectively. From Equations (12)–(15), it is easy to derive for $d > D + s_{min}$,

$$CTE_s = CTE_{CNT} \left[1 + \frac{d}{d - D} \left(\frac{CTE_{dmean}}{CTE_{CNT}} (1 + \epsilon) - 1 \right) \right] \tag{17}$$

which explains dependencies in CTE_d shown in Figure 4b,c. Furthermore, $d < D + s_{min}$ $CTE_s = 0$ because of the “floor” of s_{min} in Equations (13) and (14).

Notably for the both cases of the impregnated and the dry film, CTE's of the tunnelling contacts are almost all positive.

The change in the tunnelling contact distance causes the change in the resistances/conductances of the contacts, characterised by the thermal expansion TCRs of contacts calculated in relation of the conductivity of the undeformed contact:

$$\text{TCR}_{tunn TE} = -\frac{G_{tunn}(s_{TE}) - G_{tunn}(s)}{G_{tunn}(s) \cdot \Delta T} \quad (18)$$

This change in the tunnelling conductances will cause the change in the homogenised conductivity of the film.

Figure 5 shows distributions of tunnelling contacts TCR, caused by thermal expansion for the same random RVE realisation and CNT length of 100 μm . The positive sign of TCR corresponds to the positive sign of CTE of the tunnelling contacts (Figure 4). Qualitatively, the behaviour of the dry (Figure 5a) and impregnated (Figure 5b) films are similar, with certain differences in the detail.

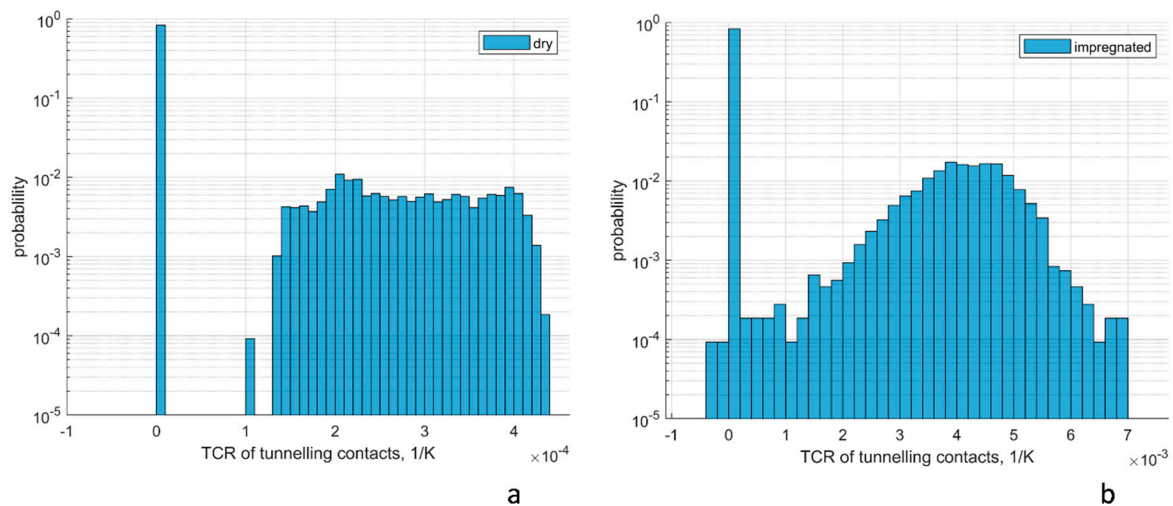


Figure 5. Distribution of TCR of tunnelling contacts caused by thermal expansion: (a) dry film; (b) impregnated film. CNT length 100 μm .

The majority of the contacts, ~80%, do not change their distance because of the limitation of the minimal distance between the CNT surfaces. This causes the large peaks of distributions with TCR equal 0. The width of the rest of the distribution is much larger for the impregnated film than for the dry one, corresponding to wider distributed CTEs (Figure 4b,c).

4. TCR of the CNT Networks and Comparative Roles of the Underlying Mechanisms

In the previous section, the temperature dependences of the resistance network elements are quantified. The nodal analysis for the conductivity homogenisation, coupled with these dependences, allows the evaluation of the comparative role of three sources for temperature dependence of the homogenised conductivity. The tunnelling conductances are under the influence of two factors: thermal excitation TCR, Equation (11); and thermal expansion TCR, Equation (14). In the coupled calculations, these two factors are assumed to influence the final TCR independently.

Such calculations were performed for randomly generated RVEs of the CNT dry films with three levels of the CNT length: 100, 250, and 500 μm , with ten random realisations per each length value.

Figure 6 shows the temperature dependence of conductivity components for dry films. There is a consistent increase in conductivity both for g_{xx} and g_{yy} with increase in temperature (Figure 6a). The calculated conductivity increase, $g_{ii}(400 \text{ K})/g_{ii}(300 \text{ K})$,

is compared with the experimental data [8] in Figure 6b. Certain differences with the experiment are seen: the conductivity increase in the experiment is the same for different CNT lengths, but in the calculations, it increases from ~ 1.15 for the length of $100 \mu\text{m}$ to ~ 1.22 for the length of $500 \mu\text{m}$. However, the calculated TCR:

$$\text{TCR} = (1 - g_{ii}(T)/g_{ii}(300 \text{ K}))/100 \text{ K} = -0.0015 \dots -0.0022 \text{ 1/K} \quad (19)$$

is close to the average TCR of -0.0012 1/K , as reported in [8], and is consistent with the values in the range $0.001\text{--}0.003 \text{ 1/K}$, measured for the aligned CNT films in [2,6,7]. We attribute the difference with the experiment to that in [8]. CNTs of very high quality (defect-free) were grown to the extent that their conductance remained ballistic even at high lengths of CNT segments. On the contrary, in our calculations we assumed average quality CNTs with defects and finite intrinsic CNT conductivity (Table 1), which led to significant CNT length dependence (Figure 3a).

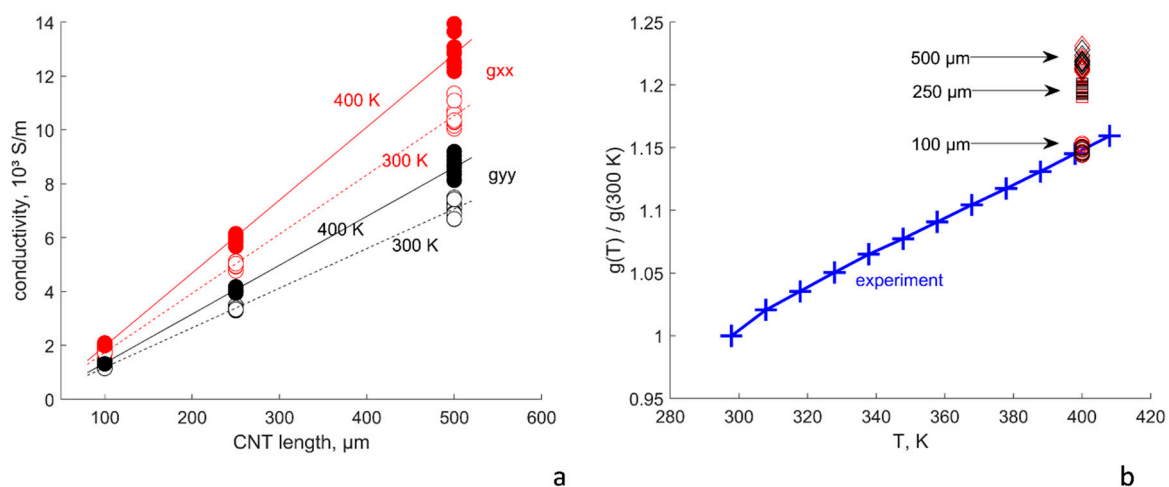


Figure 6. Temperature dependence of the dry film conductivity: (a) change in the conductivity components for different CNT length: markers—calculated values in ten random realisations, lines—linear regressions; (b) ratio $g(T)/g(300 \text{ K})$: crosses—experimental values [8], mixed g_{xx} and g_{yy} components, size of the marker corresponds to the standard deviation; calculated values at 400 K: CNT length $100 \mu\text{m}$ (circles), $250 \mu\text{m}$ (squares), $500 \mu\text{m}$ (diamonds), red markers— g_{xx} , black markers— g_{yy} .

Table 2 shows details of the TCR calculations. It shows values calculated for dry films. The difference in the conductivity values for impregnated CNT films appears only in CTE-affected cases. It is below 0.3% and is, therefore, negligible.

Data in Table 2 give comparisons of conductivity calculated for different temperature dependence mechanisms. It shows that the temperature dependence of the intrinsic CNT conductivity plays the prevailing role in the negative TCR of the homogenised resistance. Thermal expansion gives, as could be expected, positive TCR; thermal excitation gives negative TCR; both these contributions are one to two orders of magnitude smaller than that of the intrinsic conductivity.

This result is opposite to the conclusion by the authors of [8] who stated that the temperature dependence of the tunnelling resistance is of primary importance. This statement is not based not on direct measurements or modelling but instead on non-direct evaluations and reasoning. Moreover, Ref. [8] do not include in their reasoning thermal expansion of the network, nor the intrinsic resistance of the CNTs. The present calculations include all three factors and give simulation results that are consistent with experimental measurements, which gives credibility to our conclusions above.

Recently [35], it was demonstrated that the controversy of data on TCRs in the literature may be caused by the measurements taken from material that was not fully cured. This factor can also play a role in the experiment's interpretation.

Table 2. Film conductivities and TCRs, mean, and standard deviation in 10 RVE realisations, calculated for different temperature dependence mechanisms.

CNT Length		100 μm		250 μm		500 μm	
VF		0.11		0.27		0.53	
Temperature Dependency Mechanism		$g_{xx}, 10^3 \text{ S/m}$	$g_{yy}, 10^3 \text{ S/m}$	$g_{xx}, 10^3 \text{ S/m}$	$g_{yy}, 10^3 \text{ S/m}$	$g_{xx}, 10^3 \text{ S/m}$	$g_{yy}, 10^3 \text{ S/m}$
Reference conductivity at 300 K		1.76 ± 0.05	1.18 ± 0.04	4.99 ± 0.11	3.37 ± 0.06	10.5 ± 0.41	7.07 ± 0.28
Influence of thermal effects on conductivity at 400 K	only thermal expansion	1.75 ± 0.05	1.18 ± 0.03	4.96 ± 0.11	3.35 ± 0.06	10.5 ± 0.41	7.04 ± 0.30
	only thermal excitation	1.77 ± 0.05	1.19 ± 0.04	4.99 ± 0.11	3.38 ± 0.06	10.6 ± 0.41	7.08 ± 0.28
	only intrinsic	2.03 ± 0.06	1.37 ± 0.04	5.98 ± 0.15	4.05 ± 0.07	12.9 ± 0.57	8.65 ± 0.34
	ALL	2.02 ± 0.05	1.36 ± 0.04	5.96 ± 0.15	4.03 ± 0.07	12.8 ± 0.57	8.61 ± 0.34
		TCR, 10^{-3} 1/K					
Influence of thermal effects on TCR over the range 300 K–400 K	only thermal expansion	0.055 ± 0.004	0.054 ± 0.0031	0.052 ± 0.004	0.050 ± 0.0031	0.046 ± 0.005	0.050 ± 0.0063
	only thermal excitation	-0.015 ± 0.0003	-0.015 ± 0.0002	-0.015 ± 0.0002	-0.015 ± 0.0002	-0.015 ± 0.0004	-0.015 ± 0.0003
	only intrinsic	-1.53 ± 0.03	-1.52 ± 0.02	-2.00 ± 0.02	-2.01 ± 0.03	-2.22 ± 0.07	-2.23 ± 0.04
	ALL	-1.48 ± 0.03	-1.48 ± 0.02	-1.95 ± 0.03	-1.96 ± 0.03	-2.18 ± 0.07	-2.18 ± 0.04

Note: The difference of the values for dry and impregnated films is below the precision of three digits, adopted in the table, and not demonstrated.

5. Conclusions

Three phenomena define TCR of CNT networks: temperature dependence of the intrinsic conductivity of CNTs, of the tunnelling resistance of their contacts, and thermal expansion of the nanocomposite. We have investigated, via a numerical modelling, the comparative role of these phenomena in the temperature range 300–400 K for aligned CNT films, created by rolling down the forests of different length, as described in [8], and the same films impregnated by epoxy matrix. The calculated TCR in the range from -0.0015 to -0.0022 1/K is close to the experimentally observed values.

For the studied materials and studied temperature interval, the main factor affecting the TCR of the A-CNT network is the TCR of the CNTs themselves. Thermal excitation TCR of the tunnelling contacts plays the second role; influence of the film thermal expansion is marginal. The prevailing impact of the intrinsic conductivity TCR in the TCR of the film is explained by long inter-contact segments of CNTs in an A-CNT network, which define the homogenised film conductivity.

Author Contributions: Conceptualization, S.V.L., I.S.A. and S.G.A.; methodology, S.V.L., I.S.A., Q.L., Q.W. and S.G.A.; software, S.V.L., I.S.A.; validation, S.V.L. and S.G.A.; formal analysis, S.V.L. and I.S.A.; investigation, S.V.L., I.S.A. and S.G.A.; resources, S.G.A.; data curation, S.V.L.; writing—original draft preparation, S.V.L.; writing—review and editing, S.V.L., I.S.A., Q.L., Q.W. and S.G.A.; visualization, S.V.L.; supervision, S.G.A.; project administration, S.G.A.; funding acquisition, S.G.A. All authors have read and agreed to the published version of the manuscript.

Funding: This work was supported by Skoltech NGP Program, project “Multifunctional Fusion: Life-cycle enhancements via data-driven nanoengineering of advanced composite structures”.

Institutional Review Board Statement: Not applicable.

Informed Consent Statement: Not applicable.

Data Availability Statement: The raw/processed data required to reproduce these findings cannot be shared at this time as the data also forms part of an ongoing study.

Conflicts of Interest: The authors declare no conflict of interest.

Appendix A. Geometrical and Electrical Models of an A-CNT Film

The geometrical model algorithm is described in [15,16]. The “growth” algorithm uses random choice of the direction of the generated CNT path segment but with certain constraints, as described below. The n^{th} segment of a CNT is characterized by length l_{seg} , azimuthal angle φ_n , and polar angle θ_n . For the generation of an aligned assembly, the angles φ_n and θ_n are defined in relation to a Cartesian coordinate system with axis z corresponding to the average direction of the forest after rolling down, θ_{rolled} . The angles φ_n and θ_n are random values. They are first calculated as $\varphi_n = \text{rand}(0, 2\pi)$ and $\cos \theta_n = \text{randN}(1, \cos(\sigma_\theta))$, where $\text{rand}(a, b)$ is a random generator for uniform distribution on $[a, b]$, and $\text{randN}(a, \sigma)$ is a random generator for a normal distribution with mean a and standard deviation σ , and σ_θ is a characteristic polar angle deviation, which is calculated based on the length of the CNT segment and the maximal curvature. The randomness of the segment orientation is restricted by the following conditions:

- Maximal path curvature and torsion are limited: $\kappa \leq \kappa_{\text{max}}$; $\tau \leq \tau_{\text{max}}$. (see Table 1 for maximal values);
- Correlated random angles: the sequences of φ_n and θ_n pairs are auto-correlated along the CNT path, with the assumed correlation length of 100 nm.

The CNTs’ origins are placed randomly and uniformly on a plane, using a Poisson random process. Geometric periodicity is assumed: the model is confined within a representative volume element (RVE); if a CNT crosses an RVE face, then it is continued from the opposite face until the full length of the CNT is reached. The number of CNTs in the model is defined based on the prescribed volume fraction (VF).

Once an RVE is created, the geometric network of the CNT assembly is analysed for contacts between the CNTs and then transformed into the set of nodes, which are connected with electrical resistances/conductances and assigned to the tunnelling contacts, according to Equations (5)–(7), (11), and (14), and to the CNT sections between the contacts, according to Equations (4), (7), and (9). The electrical boundary conditions are periodical, with the given voltage applied to the opposite faces of the RVE. A linear system of equations (“Kirchhoff equations”) for nodal analysis is created and solved, following [36]. Homogenized conductivity tensor of the RVE is calculated, with components g_{nk} equal to the ratio of the total current, through a face n for voltage applied to faces k . The number of equations in the linear system is ~15,000. Matlab function *mldivide* is used for the solution. The reader is referred to [16,21] for a more detailed description of the procedure.

References

1. Skákalová, V.; Kaiser, A.B.; Woo, Y.-S.; Roth, S. Electronic transport in carbon nanotubes: From individual nanotubes to thin and thick networks. *Phys. Rev. B* **2006**, *74*, 085403. [CrossRef]
2. Wang, D.; Song, P.; Liu, C.; Wu, W.; Fan, S. Highly oriented carbon nanotube papers made of aligned carbon nanotubes. *Nanotechnology* **2008**, *19*, 075609. [CrossRef]
3. Karimov, K.S.; Chani, M.T.S.; Khalid, F.A. Carbon nanotubes film based temperature sensors. *Phys. E: Low-Dimens. Syst. Nanostructures* **2011**, *43*, 1701–1703. [CrossRef]
4. Mohiuddin, M.; Hoa, S. Temperature dependent electrical conductivity of CNT-PEEK composites. *Compos. Sci. Technol.* **2011**, *72*, 21–27. [CrossRef]
5. Lasater, K.L.; Thostenson, E.T. In situ thermoresistive characterization of multifunctional composites of carbon nano-tubes. *Polymer* **2012**, *53*, 5367–5374. [CrossRef]
6. Marschewski, J.; Bin In, J.; Poulikakos, D.; Grigoropoulos, C.P. Synergistic integration of Ni and vertically aligned carbon nanotubes for enhanced transport properties on flexible substrates. *Carbon* **2014**, *68*, 308–318. [CrossRef]
7. Chen, G.; Futaba, D.N.; Sakurai, S.; Yumura, M.; Hata, K. Interplay of wall number and diameter on the electrical conductivity of carbon nanotube thin films. *Carbon* **2014**, *67*, 318–325. [CrossRef]
8. Lee, J.; Stein, I.Y.; Devoe, M.E.; Lewis, D.J.; Lachman, N.; Kessler, S.S.; Buschhorn, S.T.; Wardle, B.L. Impact of carbon nano-tube length on electron transport in aligned carbon nanotube networks. *Appl. Phys. Lett.* **2015**, *106*, 053110. [CrossRef]
9. Gong, S.; Zhu, Z.H.; Li, Z. Electron tunnelling and hopping effects on the temperature coefficient of resistance of carbon nanotube/polymer nanocomposites. *Phys. Chem. Chem. Phys.* **2017**, *19*, 5113–5120. [CrossRef]

10. Gong, S.; Wang, Y.; Xiao, Z.; Li, Z.; Wang, Z.X.; Lei, R.S.; Zhu, Z.H. Effect of temperature on the electrical property of epoxy composites with carbon nanotube. *Compos. Sci. Technol.* **2017**, *149*, 48–54. [[CrossRef](#)]
11. Xiao, T.; Gong, S.; Lei, X.; Jiang, Z.; Wang, Y.; Wu, D.; Xiao, Z.; Zhu, Z.; Li, Z. High temperature response capability in carbon nanotube/polymer nanocomposites. *Compos. Sci. Technol.* **2018**, *167*, 563–570. [[CrossRef](#)]
12. Gao, F.; Mei, B.; Xu, X.; Ren, J.; Zhao, D.; Zhang, Z.; Wang, Z.; Wu, Y.; Liu, X.; Zhang, Y. Rational design of ZnMn₂O₄ nano-particles on carbon nanotubes for high-rate and durable aqueous zinc-ion batteries. *Chem. Eng. J.* **2022**, *448*, 137742. [[CrossRef](#)]
13. Zhao, D.; Zhang, Z.; Ren, J.; Xu, Y.; Xu, X.; Zhou, J.; Gao, F.; Tang, H.; Liu, S.; Wang, Z.; et al. Fe₂VO₄ nanoparticles on rGO as anode material for high-rate and durable lithium and sodium ion batteries. *Chem. Eng. J.* **2023**, *451*, 138882. [[CrossRef](#)]
14. Haghgoo, M.; Ansari, R.; Hassanzadeh-Aghdam, M.K.; Nankali, M. A novel temperature-dependent percolation model for the electrical conductivity and piezoresistive sensitivity of carbon nanotube-filled nanocomposites. *Acta Mater.* **2022**, *230*, 117870. [[CrossRef](#)]
15. Lomov, S.V.; Lee, J.L.; Wardle, B.L.; Gudkov, N.A.; Akhatov, I.S.; Abaimov, S.G. Computational description of the geometry of aligned carbon nanotubes in polymer nanocomposites. In Proceedings of the American Society for Composites—Thirty-Sixth Technical Conference on Composite Materials, Virtual Conference, 20–22 September 2021; pp. 1606–1613.
16. Gudkov, N.A.; Lomov, S.V.; Akhatov, I.S.; Abaimov, S.G. Conductive CNT-polymer nanocomposites digital twins for self-diagnostic structures: Sensitivity to CNT parameters. *Compos. Struct.* **2022**, *291*, 115617. [[CrossRef](#)]
17. Simmons, J.G. Generalized Formula for the Electric Tunnel Effect between Similar Electrodes Separated by a Thin Insulating Film. *J. Appl. Phys.* **1963**, *34*, 1793–1803. [[CrossRef](#)]
18. Matthews, N.; Hagmann, M.J.; Mayer, A. Comment: “Generalized formula for the electric tunnel effect between similar electrodes separated by a thin insulating film”. [*J. Appl. Phys.* *34*, 1793 (1963)]. *J. Appl. Phys.* **2018**, *123*, 136101. [[CrossRef](#)]
19. DeRosa, P.A.; Michalak, T. Polymer-mediated tunneling transport between carbon nanotubes in nanocomposites. *J. Nanosci. Nanotechnol.* **2014**, *14*, 3696–3702. [[CrossRef](#)] [[PubMed](#)]
20. Penazzi, G.; Carlsson, J.M.; Diedrich, C.; Olf, G.; Pecchia, A.; Frauenheim, T. Atomistic Modeling of Charge Transport across a Carbon Nanotube–Polyethylene Junction. *J. Phys. Chem. C* **2013**, *117*, 8020–8027. [[CrossRef](#)]
21. Lomov, S.V.; Gudkov, N.A.; Abaimov, S.G. Uncertainties in Electric Circuit Analysis of Anisotropic Electrical Conductivity and Piezoresistivity of Carbon Nanotube Nanocomposites. *Polymers* **2022**, *14*, 4794. [[CrossRef](#)]
22. Lee, D.H.; Lee, J.K. Initial compressional behaviour of fibre assembly. In *Objective Measurement: Applications to Product Design and Process Control*; Kawabata, S., Postle, R., Niwa, M., Eds.; The Textile Machinery Society of Japan: Osaka, Japan, 1985; pp. 613–622.
23. Lomov, S.V.; Gorbatiikh, L.; Verpoest, I. A model for the compression of a random assembly of carbon nanotubes. *Carbon* **2011**, *49*, 2079–2091. [[CrossRef](#)]
24. Gong, S.; Wu, D.; Li, Y.; Jin, M.; Xiao, T.; Wang, Y.; Xiao, Z.; Zhu, Z.; Li, Z. Temperature-independent piezoresistive sensors based on carbon nanotube/polymer nanocomposite. *Carbon* **2018**, *137*, 188–195. [[CrossRef](#)]
25. Naemi, A.; Meindl, J.D. Physical Modeling of Temperature Coefficient of Resistance for Single- and Multi-Wall Carbon Nanotube Interconnects. *IEEE Electron. Device Lett.* **2007**, *28*, 135–138. [[CrossRef](#)]
26. Naemi, A.; Meindl, J.D. Carbon nanotube interconnects. In Proceedings of the 2007 International Symposium on Physical Design, Austin, TX, USA, 18–21 March 2007; Association for Computing Machinery: Austin, TX, USA, 2007; pp. 77–84.
27. Garanin, D.A.; Chudnovsky, E.M. Thermally activated resonant magnetization tunneling in molecular magnets: Mn₁₂Ac and others. *Phys. Rev. B* **1997**, *56*, 11102–11118. [[CrossRef](#)]
28. Deng, L.; Young, R.J.; Kinloch, I.A.; Sun, R.; Zhang, G.; Noé, L.; Monthieux, M. Coefficient of thermal expansion of carbon nanotubes measured by Raman spectroscopy. *Appl. Phys. Lett.* **2014**, *104*, 051907. [[CrossRef](#)]
29. Romanov, V.S.; Lomov, S.V.; Verpoest, I.; Gorbatiikh, L. Modelling evidence of stress concentration mitigation at the micro-scale in polymer composites by the addition of carbon nanotubes. *Carbon* **2015**, *82*, 184–194. [[CrossRef](#)]
30. Liu, Q.; Lomov, S.V.; Gorbatiikh, L. Spatial distribution and orientation of nanotubes for suppression of stress concentrations optimized using genetic algorithm and finite element analysis. *Mater. Des.* **2018**, *158*, 136–146. [[CrossRef](#)]
31. Lebedev, O.; Ozerin, A.; Abaimov, S. Multiscale Numerical Modeling for Prediction of Piezoresistive Effect for Polymer Composites with a Highly Segregated Structure. *Nanomaterials* **2021**, *11*, 162. [[CrossRef](#)]
32. Matos, M.A.; Tagarielli, V.L.; Baiz-Villafranca, P.M.; Pinho, S.T. Predictions of the electro-mechanical response of conductive CNT-polymer composites. *J. Mech. Phys. Solids* **2018**, *114*, 84–96. [[CrossRef](#)]
33. Tian, W.; Chao, X.; Fu, M.; Qi, L.; Ju, L. New numerical algorithm for the periodic boundary condition for predicting the coefficients of thermal expansion of composites. *Mech. Mater.* **2021**, *154*, 103737. [[CrossRef](#)]
34. Durville, D. Contact-friction modeling within elastic beam assemblies: An application to knot tightening. *Comput. Mech.* **2012**, *49*, 687–707. [[CrossRef](#)]
35. Jafarypouria, M.; Mahato, B.; Abaimov, S.G. Separating Curing and Temperature Effects on the Temperature Coefficient of Resistance for a Single-Walled Carbon Nanotube Nanocomposite. *Polymers* **2023**, *15*, 433. [[CrossRef](#)] [[PubMed](#)]
36. Ho, C.-W.; Ruehli, A.; Brennan, P. The modified nodal approach to network analysis. *IEEE Trans. Circuits Syst.* **1975**, *22*, 504–509.

Disclaimer/Publisher’s Note: The statements, opinions and data contained in all publications are solely those of the individual author(s) and contributor(s) and not of MDPI and/or the editor(s). MDPI and/or the editor(s) disclaim responsibility for any injury to people or property resulting from any ideas, methods, instructions or products referred to in the content.